Applied Physics Express

LETTER • **OPEN ACCESS**

Phase-controllable multi-laser system with coaxially combined near-infrared and subcycle mid-infrared and THz pulsed beams

To cite this article: Yusuke Arashida *et al* 2022 *Appl. Phys. Express* **15** 092006

OPEN ACCESS

Applied Physics Express 15, 092006 (2022) LETTER

https://doi.org/10.35848/1882-0786/ac88b6

Phase-controllable multi-laser system with coaxially combined near-infrared and subcycle mid-infrared and THz pulsed beams

Yusuke Arashida†, Naoki Umeda†, Hiroyuki Mogi, Masashi Ishikawa, Akira Hatanaka, Osamu Takeuchi, Shoji Yoshida, and Hidemi Shigekawa*

Faculty of pure and applied sciences, University of Tsukuba, 305-8573, Japan

*E-mail: hidemi@ims.tsukuba.ac.jp

†Yusuke Arashida and Naoki Umeda equally contributed to this work.

Received July 8, 2022; accepted August 9, 2022; published online August 19, 2022

With the progress of infrared high-intensity pulse technology, the ultrafast control of electronic states has been attracting considerable attention. Most elementary excitations of solids have resonance energy in the mid-infrared (MIR) frequency domain. Therefore, to understand these dynamics in detail and open up new possibilities, new technological innovations are desired. In this study, we have developed a system that combines 8 fs near-infrared pulsed light with carrier envelope phase-controllable subcycle MIR and THz pulsed lights. This technology has produced a new method that enables the analysis of phase-sensitive phenomena in the near-infrared to far-infrared region.

Supplementary material for this article is available online

With the innovation of femtosecond technology, attempts to understand and control electronic states in materials and devices in the ultrafast time domain are being actively promoted.[1–6] Among them, the attractive dynamics of physical properties exhibited by elementary excitations (e.g. excitons, phonons, superconducting quasiparticles, charge density waves) existing in the energy region of 1–200 meV are of great interest.[5,7–17] To elucidate these physical characteristics, many THz and mid-infrared (MIR) light sources have been developed,[18,19] and recently, electric field-driven phenomena, as well as photon-driven phenomena, have been reported.[3,16] To understand these phenomena in the ultrafast region more spectroscopically, in addition to the introduction of a wideband MIR pulse, a new technological innovation is desired. One attractive direction is to use a combination of carrier envelope phase (CEP)-controlled subcycle electric fields, which have recently become stable and usable.

In this study, we have developed a system that combines 8 fs near-infrared (NIR) pulsed light with CEP-controllable subcycle MIR (1 cycle ∼50 fs, 30 THz bandwidth) and THz (1 cycle ∼1 ps, 1 THz bandwidth) pulsed lights. These three beams can be used in a coaxial arrangement while maintaining their respective band conditions. The combination of the monopolar subcycle electric fields enables the analysis of ultrafast quantum processes under well-controlled conditions produced by an electric-field-drive method, which opens up new possibilities. For example, since the pulse width of the MIR light is sufficiently smaller than the THz pulse width, a THz pump and MIR probe method makes it possible to analyze quasiparticle dynamics, which are sensitive to the THz-drive phase condition.

Furthermore, the NIR pulse can be used to characterize the MIR light waveform by electro-optic sampling. That is, since both the real and imaginary parts of permittivity can be found, and thereby, the complex refractive index in the wideband MIR region can be obtained, all the information probed by the general optical measurement can be analyzed with this system.[20] In addition, the NIR pulse can be used as a probe to measure the carrier dynamics near the bandgap edge using the pump–probe method based on absorption bleaching.[21]

In actual experiments, a pump–probe optical system that uses MIR and THz lights generated by wavelength conversion is more complex than a system where only visible/NIR lasers are used. The coaxial three-beam optical system established in this study simplifies the optical setup. Therefore, combining this system with analytical techniques performed under, for example, low-temperature and ultra-high-vacuum conditions will be relatively straightforward, further accelerating research on ultrafast physical properties.[15,22–29]

Figure 1(a) shows a schematic diagram of the developed system based on an optical parametric chirped pulse amplifier (Venteon OPCPA).[30] In this system, the wideband light output (650–1050 nm) of Ti:S oscillator is first divided into two parts, one with a center wavelength of 1032 nm, and the other with a wavelength range of 650–1020 nm. Subsequently, the former light (center wavelength 1032 nm) is amplified by fiber amplifiers to 90 W, which is divided into two beams of 70 and 20 W. The 20 W light is used as the NIR2 light beam shown in Fig. 1(a). On the other hand, NIR1 (4.0 W, 650 to 950 nm, pulse width 8.2 fs, repetition frequency 4 MHz) shown in Fig. 1(a) is produced by passing the latter light (650–1020 nm) through a non-collinear optical parametric amplifier twice using the second harmonic generation (SHG) of the 70 W light as the pump. The spectrum of NIR1 and its intensity waveform obtained by reconstructing it by the dispersion-scan method (D-scan, sphere photonics) are shown in Figs. 1(b) and 1(c), respectively.

The NIR1 pulse is divided into two beams, one for MIR pulse generation [upper path in Fig. 1(a)] and the other for electric-field waveform sampling (lower path in the figure). The subcycle MIR pulses are generated by injecting the NIR1 pulse into a GaSe crystal with a thickness of 30 μm through lens f_1 with a focal length of 150 mm.[30] Using the incident angle of 41° from the c-axis, a wideband MIR pulse is obtained by the optical rectification effect.[19] The generated

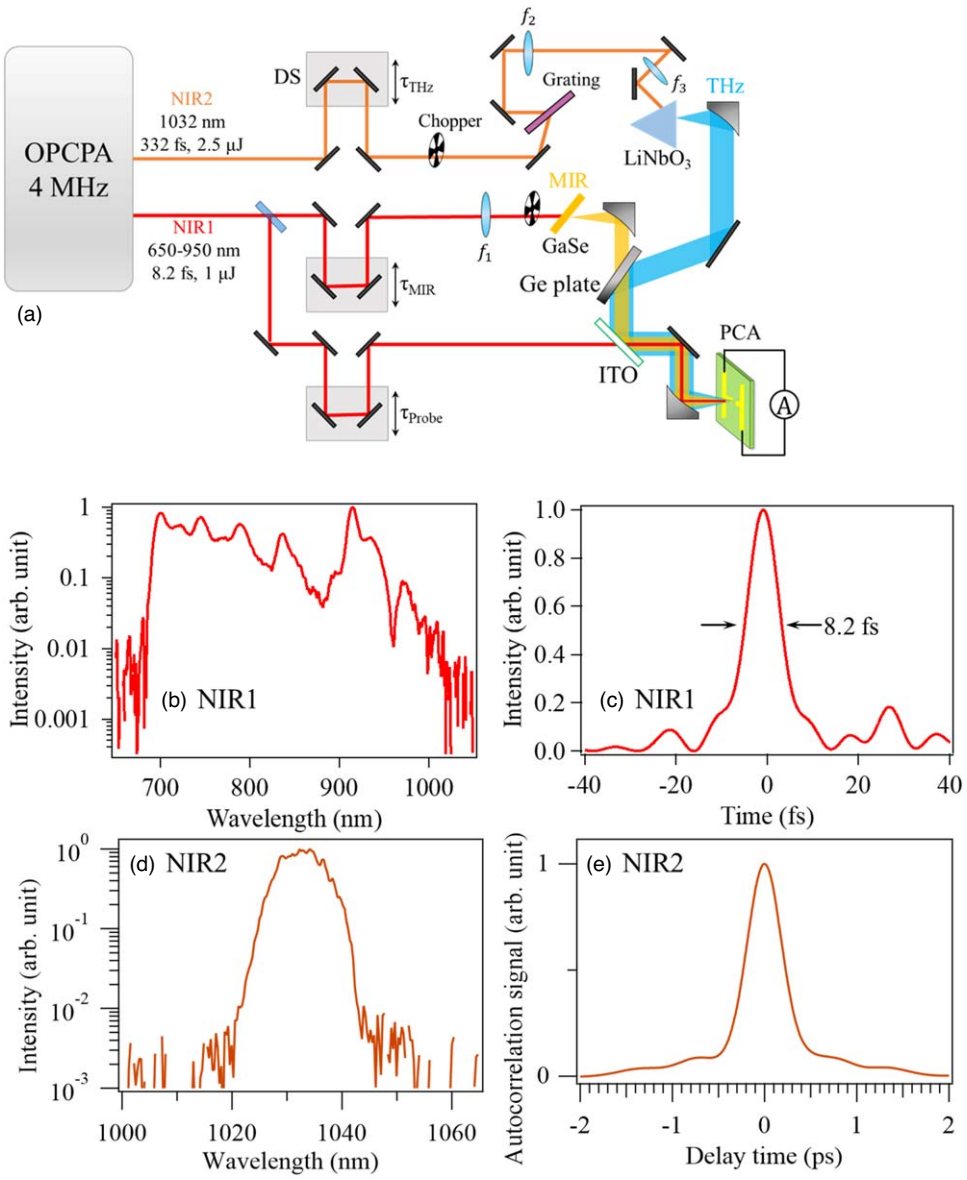

Fig. 1. (Color online) (a) Schematic diagram of the developed system (see Figs. S1 to S3 for more detail, available online at stacks.iop.org/APEX/15/092006/mmedia). f_1, f_2, f_3: lenses with focal lengths of 150 mm, 200 mm, and 125 mm, respectively, DS: delay stage, ITO: fused silica plate (thickness = 1 mm) coated with indium tin oxide, and PCA: photoconductive antenna. (b) (c) NIR1 spectrum obtained by PCA and its intensity waveform reconstructed by D-scan (sphere photonics) method. (d) (e) NIR2 spectrum and its autocorrelation function using SHG.

MIR light is collimated by an off-axis parabolic OAP with a focal length of 50 mm and transmitted into a Ge plate (undoped, 0.5 mm thickness) at an incident angle of ~70° to remove the fundamental wave. Since Ge shows a high absorption coefficient in the NIR/visible region with a wavelength of less than 1.5 μm, the NIR pulse, which is the fundamental wave of the laser, can be removed without being transmitted.

On the other hand, the subcycle THz pulses are generated by irradiating NIR2 into the $LiNbO_3$ crystal by the tilt-pulse-front method.[18] The primary diffracted light from a grating (1600 mm^{-1}) is incident on the crystal using two lenses with focal lengths of 200 mm (f_2) and 125 mm (f_3). The THz pulses generated by the optical rectification effect is collimated with a parabolic mirror with a focal length of 25 mm. After that, as shown in Fig. 1(a), the MIR and THz lights are combined in a coaxial arrangement by reflecting the s-polarized THz light on the Ge substrate that transmits the MIR light. At this time, the polarizations of the MIR and THz lights are orthogonal. Next, the merged beams are reflected by a quartz substrate with an ITO coating (IQP-501, UQG Optics), and the NIR1 beam in the lower path is transmitted from the opposite side to coaxially combine it with the THz and MIR lights. For the substrate of ITO, quartz with a thickness of 1 mm is used to reduce the dispersion of the NIR1 pulse. Combining the three beams in this manner makes it possible to simplify the optical system of pump–probe spectroscopy in the MIR region, which is effective in experiments with analytical techniques performed under low-temperature and ultrahigh-vacuum conditions as described above.

The combined beam was focused on a photoconductive antenna (PCA: BATOP PCA-40-05-10-1060-0) using an off-axis parabolic mirror with a focal length of 50 mm, and the electric field waveform was evaluated. Sampling was performed by sweeping the delay time of NIR1 with respect to the MIR and THz lights. The delay times of the NIR1, MIR, and THz lights are controlled by independent delay stages,

and the delay time between the MIR and NIR1 lights and that between the MIR and THz lights are expressed as τ_{NM} and τ_{MT} in the following part, respectively.

Figure 2 shows the electric field waveforms measured using the PCA. As shown in Fig. 2(a), the MIR waveform was confirmed to have a subcycle that oscillated with a wavelength of about 50 fs. As shown in Fig. 2(b), its Fourier spectrum has a center frequency of 20 THz and a bandwidth of 20 THz or more. The bandwidth of MIR is determined by the phase matching of GaSe.[19] The dip near 7 THz is considered to be due to the absorption characteristics of GaSe and Ge.[19,31] Note that the actual bandwidth of the MIR is broader than 20 THz if EO sampling or a different type of PCA is used to measure.[30] The electric field of the THz waveform is also a subcycle and close to monopolar, as shown in Fig. 2(c). Its Fourier spectrum has a center frequency of 1 THz and a bandwidth of about 1.5 THz, as shown in Fig. 2(d). The THz band structure depends on the NIR2 pulse structure.

By combining the MIR and THz electric fields, for example, as shown in Fig. 3(a), it becomes possible to analyze the quantum processes while they are dynamically driven and controlled. Figure 3(b) shows the waveform of the combined beam of the MIR and THz electric fields. The measurement was performed for $\tau_{TM} = 0$, 275, and 500 fs by directing the measurement axis of the optical conduction antenna to the middle of the polarization directions of the MIR and THz electric fields. The high-speed modulation by the MIR electric field is manifested in the slow change in electric field with a period of 1 ps. τ_{TM} can be easily changed by adjusting the delay stage. That is, it is possible to irradiate the MIR pulse at any desired phase position of the THz electric field during its irradiation of the sample and perform a time-resolved measurement. Using this system, a new spectroscopic study of the ultrafast electric-field-driven phenomena produced by the attractive quasiparticles in solids will be realized.

In this system, phase control of the MIR electric field is also important. The generation of MIR light using a GaSe crystal and its phase control are realized by adjusting the superposition of the two types of phase matching conditions, Type 1 and Type 2.[32] The effective nonlinear coefficient d_{eff} is $d_{eff} \propto d_{22}\cos\theta\cos3\phi_{GaSe}$ for Type 1 and $d_{eff} \propto d_{22}\cos^2\theta\sin3\phi_{GaSe}$ for Type 2,[33,34] where d_{22} is the second order susceptibility tensor, θ is the incident angle of the laser, and ϕ_{GaSe} is the azimuth angle. The ratio of Type 1 to Type 2 can be controlled by changing the in-plane crystal axis direction. As an example, Figs. 3(c) and 3(d) show the results of reversing the polarity of the MIR electric field to show the high controllability of the combined beams. Setting $\phi_{GaSe} = 0°$ and 60°, we can invert the polarity of the subcycle MIR electric field with the Type 2 component being suppressed. Using the proposed system, it will be possible to advance the understanding of and control of non-equilibrium electrons in solids.[3,35] Further improvement of the control of tunnel phenomena in metal nanostructures in the ultrafast region is also expected.[25,29,36,37]

Figure 4 shows the stability of the electric field waveform, which demonstrates its usefulness for measuring physical properties. Figure 4(a) shows the measurement results of the combined waveform every 2 min for 3 h. The blue and green parts are the negative and positive regions of the THz electric field, respectively. The sharp change near the delay time of 0 fs is the contribution of the MIR electric field, which is stably located in the green part where the intensity of the THz is positive.

To evaluate the relative time difference τ_{TM} between the MIR and THz electric fields, τ_{TM} was extracted by fitting the waveform at each time with the function $E(t, \tau_{MT}) = E_{MIR}(t - \tau_{MT})$-$E_{THz}(t)$. Here, $E_{MIR}(t)$ and $E_{THz}(t)$ are waveforms obtained in advance by measuring the MIR and THz electric fields independently. The results are shown in Fig. 4(b). The initial value of τ_{TM} is about 6 fs, which changed only by about −3 fs in 3 h. The changes were 16 fs for the peak-to-peak value and 3.9 fs for the standard deviation. This means that the central time of the MIR electric field is locked with an accuracy of 2% or better for one cycle of the THz electric field. Namely, a new system that enables the analysis of phase-sensitive phenomena in the NIR to the far-infrared region has been realized.

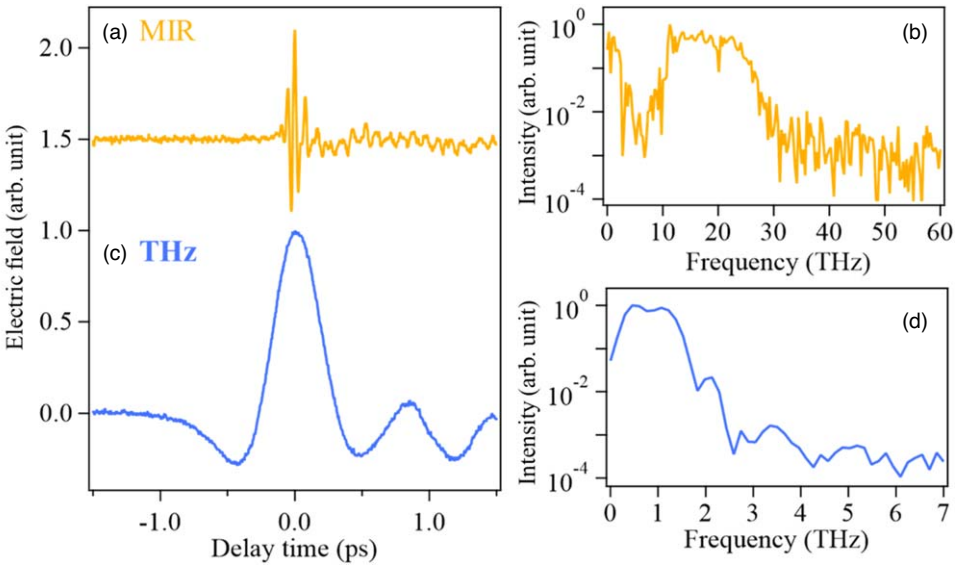

Fig. 2. (Color online) (a) Waveform of MIR electric field and (b) its Fourier spectrum. (c) Waveform of THz electric field and (d) its Fourier spectrum. All waveforms were measured using the PCA.

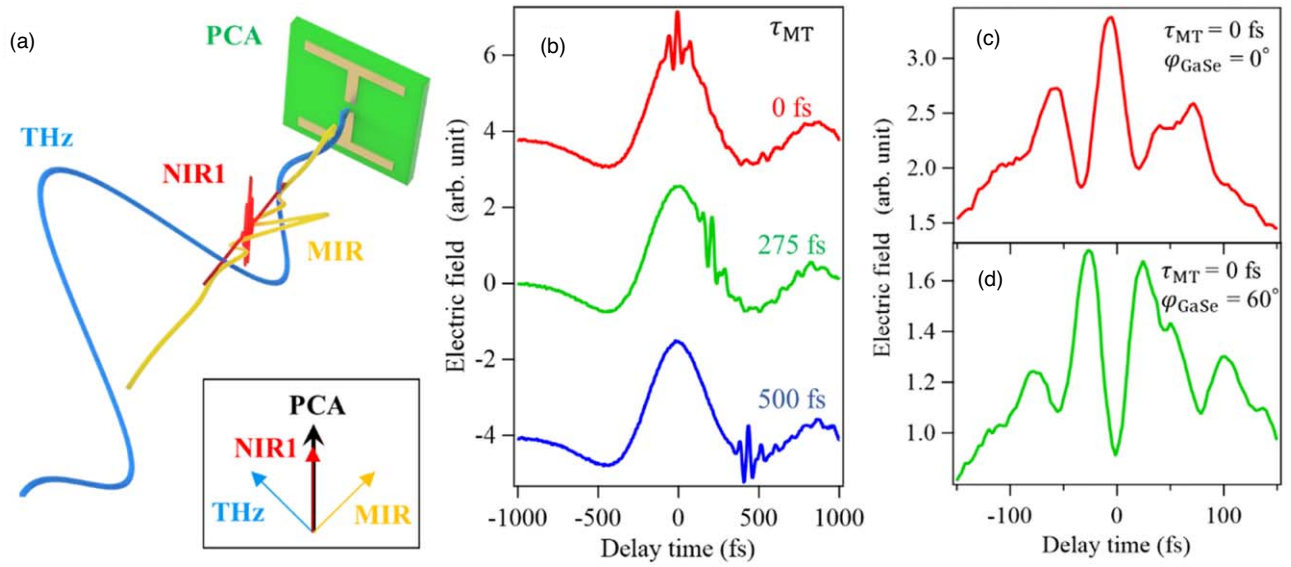

Fig. 3. (Color online) (a) Schematic diagram of the electric field waveform measurement of the three combined beams. (b) Waveform of the combined beams of the MIR and THz electric fields obtained by changing the delay time τ_{MT} between them. (c) (d) Control of the MIR electric field polarity at $\tau_{MT} = 0$ fs by setting the in-plane azimuths of the GaSe crystal to 0° and 60°, respectively.

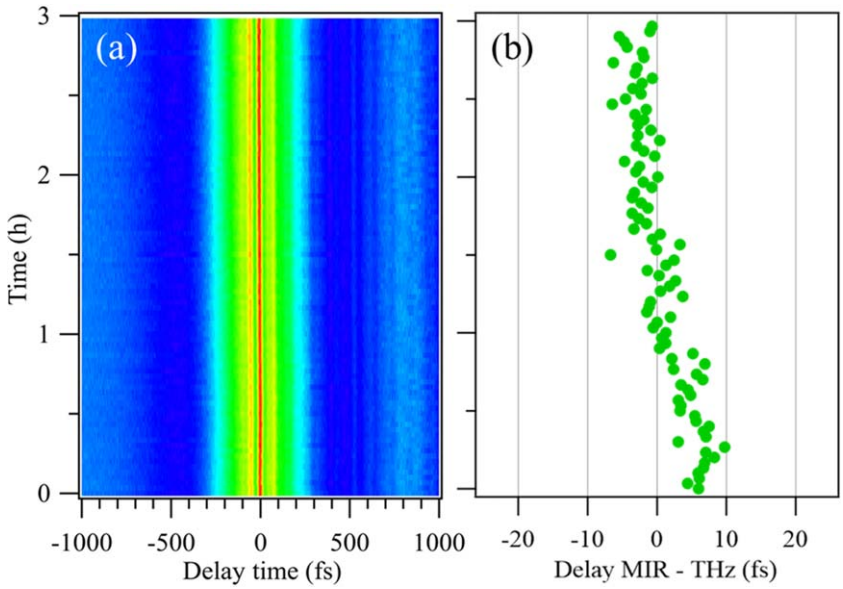

Fig. 4. (Color online) Long-term stability of the combined electric field waveform. (a) Electric field waveform measured every 2 min. The color represents the value of the electric field (a.u.). (b) Difference in delay time between MIR and THz electric fields as a function of time.

In conclusion, as a new method that makes it possible to understand and control the dynamics in the ultrahigh-speed region of a condensed system, we have realized a new system in which CEP-controlled wideband subcycle MIR (1 cycle: 50 fs) and THz (1 cycle: 1 ps) electric fields are coaxially combined. First, by using Brewster's angle of the crystal, the MIR and THz lights are combined while maintaining the band. These two beams are also combined with NIR pulsed light (8 fs) using an ITO-coated quartz beam splitter. This technology has created a new system that enables the analysis of phase-sensitive phenomena in the NIR to far-infrared region. Since the pulse width of the MIR light is sufficiently smaller than a quarter of the THz pulse width, the combination of both electric fields provides a new method of measuring the dynamics of quantum processes, such as electric-field-driven quasiparticle phenomena, while controlling them.[33] Moreover, since both the real and the imaginary parts of permittivity can be found, and thereby, the complex refractive index in the wideband MIR region can be obtained, all the information produced by the optical measurement in this region can be probed with this system. The simplified handling system with the coaxial beam is expected to have a wide range of practical applications because it is relatively easy to combine the optical system with ultralow-temperature and ultrahigh-vacuum technologies.

Acknowledgments We acknowledge the financial support of a Grant-in-Aid for Scientific Research (17H06088, 20H00341) from Japan Society for the Promotion of Science.

1) T. Kampfrath, K. Tanaka, and K. A. Nelson, Nat. Photon. **7**, 680 (2013).
2) D. N. Basov, R. D. Averitt, D. Marel, M. Dressel, and K. Haule, Rev. Mod. Phys. **83**, 471 (2011).
3) O. Schubert et al., Nat. Photon. **8**, 119 (2014).
4) R. Matsunaga, N. Tsuji, H. Fujita, A. Sugioka, K. Makise, Y. Uzawa, H. Terai, Z. Wang, H. Aoki, and R. Shimano, Science **345**, 1145 (2014).

5) H. Hirori, K. Shinokita, M. Shirai, S. Tani, Y. Kadoya, and K. Tanaka, Nat. Commun. **2**, 594 (2011).
6) T. Oka and S. Kitamura, Annu. Rev. Condens. Matter Phys. **10**, 387 (2019).
7) C. Giannetti, M. Capone, D. Fausti, M. Fabrizio, and D. Mihailovic, Adv. Phys. **65**, 58 (2016).
8) D. Fausti, R. I. Tobey, N. Dean, S. Kaiser, A. Dienst, M. C. Hoffmann, S. Pyon, T. Takayama, H. Takagi, and A. Cavalleri, Science **331**, 189 (2011).
9) G. Günter et al., Nature **458**, 178 (2009).
10) R. Mankowsky, A. von Hoegen, M. Först, and A. Cavalleri, Phys. Rev. Lett. **118**, 1 (2017).
11) C. Vicario, C. Ruchert, F. Ardana-Lamas, P. M. Derlet, B. Tudu, J. Luning, and C. P. Hauri, Nat. Photon. **7**, 720 (2013).
12) B. Zaks, R. B. Liu, and M. S. Sherwin, Nature **483**, 580 (2012).
13) S. R. Tauchert et al., Nature **602**, 73 (2022).
14) P. Gaal, W. Kuehn, K. Reimann, M. Woerner, T. Elsaesser, and R. Hey, Nature **450**, 1210 (2007).
15) Y. H. Wang, H. Steinberg, P. Jarillo-Herrero, and N. Gedik, Sience **342**, 453 (2013).
16) J. W. McIver, B. Schulte, F. U. Stein, T. Matsuyama, G. Jotzu, G. Meier, and A. Cavalleri, Nat. Phys. **16**, 38 (2020).
17) T. Rohwer et al., Nature **471**, 490 (2011).
18) H. Hirori, A. Doi, F. Blanchard, and K. Tanaka, Appl. Phys. Lett. **98**, 091106 (2011).
19) C. Kübler, R. Huber, and A. Leitenstorfer, Semicond. Sci. Technol. **20**, S128 (2005).
20) A. Leitenstorfer, S. Hunsche, J. Shah, M. C. Nuss, and W. Knox, Appl. Phys. Lett. **74**, 1516 (1999).
21) Z. Chi, H. Chen, Q. Zhao, and Y. X. Weng, J. Chem. Phys. **151**, 114704 (2019).
22) J. Reimann et al., Nature **562**, 396 (2018).
23) G. T. Noe et al., Opt. Express **24**, 30328 (2016).
24) C. Kealhofer, W. Schneider, D. Ehberger, A. Ryabov, F. Krausz, and P. Baum, Science **352**, 429 (2016).
25) G. Herink, D. R. Solli, M. Gulde, and C. Ropers, Nature **483**, 190 (2012).
26) M. Hada, D. Yamaguchi, T. Ishikawa, T. Sawa, K. Tsuruta, K. Ishikawa, S. Koshihara, Y. Hayashi, and T. Kato, Nat. Commun. **10**, 4159 (2019).
27) J. G. Horstmann, H. Böckmann, B. Wit, F. Kurtz, G. Storeck, and C. Ropers, Nature **583**, 232 (2020).
28) M. Eisele, T. L. Cocker, M. A. Huber, M. Plankl, L. Viti, D. Ercolani, L. Sorba, M. S. Vitiello, and R. Huber, Nat. Photon. **8**, 841 (2014).
29) S. Yoshida, Y. Arashida, H. Hirori, T. Tachizaki, A. Taninaka, H. Ueno, O. Takeuchi, and H. Shigekawa, ACS Photon. **8**, 315 (2021).
30) K. Yoshioka, I. Igarashi, S. Yoshiada, Y. Arashida, I. Katayama, J. Takeda, and H. Shigekawa, Opt. Lett. **44**, 5350 (2019).
31) S. C. Shen, C. J. Fang, M. Cardona, and L. Genzel, Phys. Rev. B **22**, 2913 (1980).
32) C. Gaida et al., Light: Sci. Appl. **7**, 94 (2018).
33) K. R. Allakhverdiev, M. Ö. Yetis, S. Özbek, T. K. Baykara, and E. Y. Salaev, Laser Phys. **19**, 1092 (2009).
34) J. Mei, K. Zhong, M. Wang, Y. Liu, D. Xu, W. Shi, Y. Wang, J. Yao, R. A. Norwood, and N. Peyghambarian, Opt. Express **24**, 23368 (2016).
35) R. Mankowsky, M. Först, and A. Cavalleri, Reports Prog. Phys. **79**, 64503 (2016).
36) T. L. Cocker, V. Jelic, M. Gupta, S. J. Molesky, J. A. J. Burgess, G. De Los Reyes, L. V. Titova, Y. Y. Tsui, M. R. Freeman, and F. A. Hegmann, Nat. Photon. **7**, 620 (2013).
37) T. Rybka, M. Ludwig, M. F. Schmalz, V. Knittel, D. Brida, and A. Leitenstorfer, Nat. Photon. **10**, 667 (2016).